Journal of Hydrology 517 (2014) 1019–1034

Contents lists available at ScienceDirect

Journal of Hydrology

journal homepage: www.elsevier.com/locate/jhydrol

Application of a stochastic weather generator to assess climate change impacts in a semi-arid climate: The Upper Indus Basin

N. Forsythe [a,*], H.J. Fowler [a], S. Blenkinsop [a], A. Burton [a], C.G. Kilsby [a], D.R. Archer [b], C. Harpham [c], M.Z. Hashmi [d]

[a] Water Resources Systems Research Laboratory (WRSRL), School of Civil Engineering and Geosciences, Newcastle University, UK
[b] JBA Consulting Engineers and Scientists, Skipton, UK
[c] Climatic Research Unit (CRU), School of Environmental Science, University of East Anglia, UK
[d] Global Change Impact Studies Centre (GCISC), National Centre for Physics Complex (NCP), Near Quaid-i-Azam University Campus, Shahdra Valley Road, Islamabad, Pakistan

ARTICLE INFO

Article history:
Received 3 March 2014
Received in revised form 28 May 2014
Accepted 21 June 2014
Available online 28 June 2014
This manuscript was handled by Konstantine P. Georgakakos, Editor-in-Chief, with the assistance of Emmanouil N. Anagnostou, Associate Editor

Keywords:
Weather generator
Indus Basin
Downscaling
Climate change

SUMMARY

Assessing local climate change impacts requires downscaling from Global Climate Model simulations. Here, a stochastic rainfall model (RainSim) combined with a rainfall conditioned weather generator (CRU WG) have been successfully applied in a semi-arid mountain climate, for part of the Upper Indus Basin (UIB), for point stations at a daily time-step to explore climate change impacts. Validation of the simulated time-series against observations (1961–1990) demonstrated the models' skill in reproducing climatological means of core variables with monthly RMSE of <2.0 mm for precipitation and $\leqslant$0.4 °C for mean temperature and daily temperature range. This level of performance is impressive given complexity of climate processes operating in this mountainous context at the boundary between monsoonal and mid-latitude (westerly) weather systems. Of equal importance the model captures well the observed interannual variability as quantified by the first and last decile of 30-year climatic periods.

Differences between a control (1961–1990) and future (2071–2100) regional climate model (RCM) time-slice experiment were then used to provide change factors which could be applied within the rainfall and weather models to produce perturbed 'future' weather time-series. These project year-round increases in precipitation (maximum seasonal mean change:+27%, annual mean change: +18%) with increased intensity in the wettest months (February, March, April) and year-round increases in mean temperature (annual mean +4.8 °C). Climatic constraints on the productivity of natural resource-dependent systems were also assessed using relevant indices from the European Climate Assessment (ECA) and indicate potential future risk to water resources and local agriculture.

However, the uniformity of projected temperature increases is in stark contrast to recent seasonally asymmetrical trends in observations, so an alternative scenario of extrapolated trends was also explored. We conclude that interannual variability in climate will continue to have the dominant impact on water resources management whichever trajectory is followed. This demonstrates the need for sophisticated downscaling methods which can evaluate changes in variability and sequencing of events to explore climate change impacts in this region.

1. Introduction

The Upper Indus Basin (UIB) covers a vast expanse of high-mountain Asia. Its water resources are of the utmost importance to the wellbeing of Pakistan. Water from the Indus and its tributaries is the dominant source for Pakistan's irrigation, domestic consumption and hydropower demands (Archer et al., 2010). Agricultural production from irrigated land in the Indus Basin provides 85% of cereal grain (wheat, rice) harvests as well as all sugar production and accounts for 45% of the total labour force in Pakistan. The area is also important for hydropower generation: the Tarbela dam alone supplies nearly 20% of national electricity demand.

Thus the Indus River is the lifeblood of Pakistan, and without its contribution, Pakistan's existing problems of food security and electrical load-shedding would be much greater. Present water resource management challenges in the UIB are primarily due to the considerable interannual variability in river flows and in the timing of the rising limb of the meltwater-driven hydrograph.

* Corresponding author.
E-mail address: nathan.forsythe@ncl.ac.uk (N. Forsythe).

http://dx.doi.org/10.1016/j.jhydrol.2014.06.031
0022-1694/

While in the future water stress in Pakistan will above all be driven by high demographic growth (Archer et al., 2010), hydro-climatological variability will exacerbate resource management challenges: adaptation measures adequate to cope with mean changes in water availability may be overwhelmed by acute conditions in dry, low-flow years.

Given its national and regional importance, prospects for water resources in the UIB in the coming decades are a matter of great concern (Barnett et al., 2005), particularly in downstream areas i.e. below the Tarbela reservoir. To assess likely future resource availability, there is a need for climate scenarios, the primary sources of which are projections from General Circulation Models (GCMs). Christensen et al. (2007) summarised the recent literature and suggest:

- warming greater than the global mean increase in both Central Asia and the Tibetan Plateau (nearly 4 °C of warming by 2100). More recent work by Ozturk et al. (2012) using a single regional climate model (RCM) has projected seasonal temperature increases ranging from 3 °C to 8 °C for the region;
- increased precipitation across much of Asia, including the Tibetan Plateau, during the northern hemisphere (“boreal”) winter. Ozturk et al. (2012) also found moderate increases in cold season precipitation over the UIB, albeit with decreasing precipitation in adjacent regions;
- decreased boreal summer precipitation in Central Asia and simultaneous decreases in “monsoonal flows” and large-scale tropical circulation.

The recently released draft IPCC 5th Assessment Report confirms that the new generation of GCMs (CMIP5) project changes in South Asian summer precipitation consistent with those used in AR4 (Christensen et al., 2007) although there is large model scatter with regards to projections of South Asian winter precipitation. Additionally, projected temperature change remains higher in South Asia and the Tibetan Plateau than for the global mean in the CMIP5 ensemble.

However, local changes could exhibit significant departures from regional trends, in part because of complex topography (Christensen et al., 2007); this is particularly the case in the UIB. Due to computational limitations, the spatial resolution of GCMs is relatively coarse (~150–300 km), although some higher resolution GCMs exist (~60 km). Hydrological impact studies, however, are carried out at much finer spatial scales. Thus, GCM outputs must be downscaled to an adequately fine spatial resolution and corrected for their inherent biases. A variety of downscaling techniques exist which have been comprehensively reviewed (e.g. Fowler et al., 2007) and can be broadly grouped into two categories:

(i) statistical downscaling, which incorporates a range of techniques, many drawing upon identified relationships between “predictors” of local climate and local climate variables (predictands). A commonly used method is the simple “delta change” approach where relative changes between ‘control’ and ‘future’ GCM runs are applied to time-series of local observations;
(ii) dynamical downscaling, in which a finer spatial resolution Regional Climate Model (RCM: ~25–50 km) is run over a limited spatial domain using GCM outputs as boundary conditions (see Rummukainen (2010)).

There is very little information on local-scale projections for the UIB due to limited downscaling studies over Asian sub-regions. GCM experiments (e.g. Rangwala et al., 2010) suggest elevation dependency – i.e. higher warming rates with increasing elevation – and strong potential snow cover-albedo feedbacks (Rangwala and Miller, 2012). Furthermore, even the higher spatial resolution provided by RCMs is insufficient for assessing the local-scale impacts of climate change in complex topography and so RCM outputs are normally subjected to further, statistical, downscaling. Previous studies in the Upper Indus (e.g. Akhtar et al., 2008; Immerzeel et al., 2008; Bocchiola et al., 2011) have generally applied the delta change approach to local climate observations. However, this method provides no simulation of changes to inter-annual variability or the sequencing of dry and wet periods, unlike other methods such as weather generators. Interannual variability of summer runoff in key UIB tributaries is large and can exceed 25% (Forsythe et al., 2012a); this may be of equal or greater importance than change to mean conditions in determining future water availability for irrigated agriculture.

In this study, we develop a point-based stochastic weather generator (WG) downscaling method (Kilsby et al., 2007) for three stations in the UIB. This WG approach has been previously used for the UK climate projections (UKCP09; Jones et al., 2009). It has also been used outside the UK for climate change impact assessments in Europe, e.g. the Dommel catchment in the Netherlands (van Vliet et al., 2012; Visser et al., 2012), and the Geer basin in Belgium (Burton et al., 2010; Blenkinsop et al., 2013; Goderniaux et al., 2011). This paper documents one of only a handful of integrated implementations of the WG approach outside Europe. It is also the first implementation of the WG in a semi-arid climate regime with substantial monsoonal influence. This paper has two aims: (1) to demonstrate the performance of the WG approach in a semi-arid climate, and (2) to perform an initial exploration of the range of potential impacts on UIB water resources and food security resulting from plausible climate trajectories. This paper therefore marks an important milestone in the development of the WG downscaling technique and establishment of its applicability and utility in broader climatic contexts.

The paper is structured as follows. Section 2 provides a summary of the data sources and Section 3 details the WG methodology and analysis methods used in this study. Section 4 provides an assessment of the performance of the WG methodology for three point locations in the semi-arid UIB climate. Section 5 then provides downscaled future climate scenarios for the same three locations. Section 6 discusses the results in the context of the literature and provides some brief conclusions and future directions.

2. Data

2.1. Observations and reanalyses

The Upper Indus Basin (UIB) covers a vast expanse of high-mountain Asia, mainly located in northern Pakistan. Fig. 1 presents a map of the UIB showing tributary catchment boundaries and positioning of data sources (local observations, meteorological reanalysis and RCM simulations) used in this study.

We use daily maximum and minimum temperature and precipitation data from the Pakistan Meteorological Department (PMD) for three UIB stations: Gilgit (1460 m asl), Skardu (2210 m asl) and Astore (2394 m asl). Record lengths vary but data is available for all stations from 1961 to 2000. These point locations are not representative of whole catchment conditions due to their relatively low elevations, but are used due to their substantial record length and the proven coherence between the individual stations (Archer, 2003, 2004; Fowler and Archer, 2006). Specifically Fowler and Archer (2006) performed “double mass curve analysis” between the stations used here. Additionally prior to application of the weather generator in this study, the data from each station were tested for homogeneity following the method prescribed for the “European Climate Analysis & Dataset” (KNMI, 2012). The “standard normal homogeneity test,” Buishand range test, Pettit

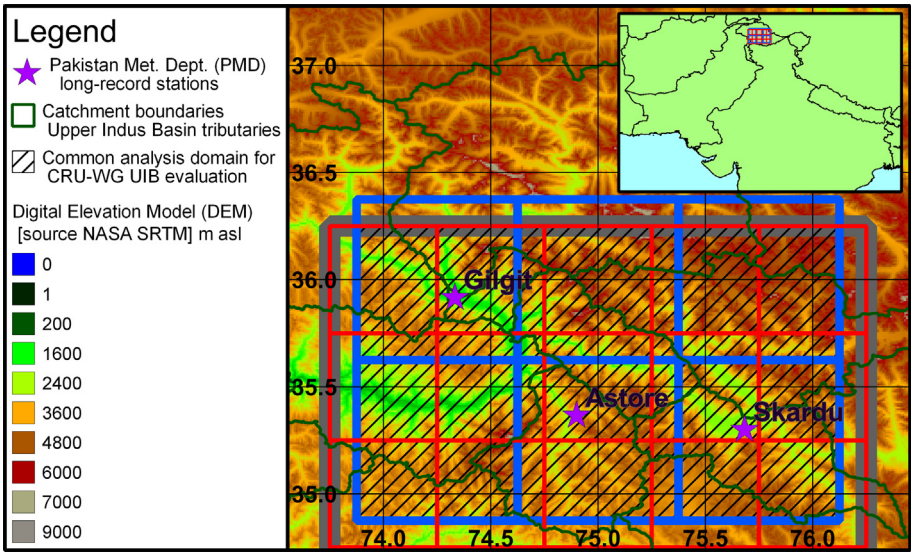

Fig. 1. Map of the study area within the UIB showing tributary catchment boundaries and positioning of data sources (local observations, meteorological reanalysis and RCM simulations). Squares show grid cell footprints for meteorological reanalysis and RCM simulations: (i) large square, thick gray boundary shows ERA-40 reanalysis; (ii) medium squares, blue boundary shows ERA-Interim; and (iii) small squares, thin red boundary shows PRECIS RCM as driven by ERA-40 reanalysis or HadAM3P GCM. Underlying elevation data (from which catchment boundaries and river courses are derived) are from NASA "shuttle radar topography mission" (SRTM) in m asl. Areal averages are calculated over a domain circumscribed by selected ERA-Interim and PRECIS grid cells (73.875E to 76.125E, 34.875 N to 36.25 N) shown with black hashing. (For interpretation of the references to colour in this figure legend, the reader is referred to the web version of this article.)

test and Von Neumann ratio test (Wijngaard et al., 2003) were performed for the primary variables, i.e. annual total precipitation and annual mean temperature, with no rejections of the null hypothesis of homogeneity at the 1% level for the 1961–1990 reference period. Furthermore, they provide meaningful indicators of catchment-scale inputs to the hydrological system when used for flow forecasts (Archer, 2003; Archer and Fowler, 2008).

We also use meteorological reanalysis products as a spatial comparison to our point observations: (i) ERA-40 (Uppala et al., 2005) for 1957–2002 at 2.5 decimal degree horizontal resolution; (ii) ERA-Interim (Dee et al., 2011) for 1979- present at 0.75 decimal degree horizontal resolution. As ERA-Interim covers the "modern satellite" epoch, the assimilated data is substantially less heterogeneous than that used by ERA-40 and thus unsurprisingly, key measures (moisture transport, energy balance) show superior performance by ERA-Interim compared to ERA-40 (Berrisford et al., 2011; Betts et al., 2009).

2.2. Available RCM data

One of the most important elements in dynamical downscaling is the GCM boundary conditions used to drive the RCM (Jacob et al., 2007; Liang et al., 2008; Pan et al., 2001). Here we use PRECIS (Jones et al., 2004) – a version of the UK Met Office Hadley Centre HadRM3 RCM – driven by the atmosphere-only GCM, HadAM3P (Pope et al., 2000). Previous studies have identified systematic biases and misrepresentations in HadAM3P results, e.g. excessively high pressures at low latitudes and seasonal shifts in the timing and magnitude of African and Asian tropical rainfall (Pope et al., 2000), and weaker simulation of the 'Azores High' (Anagnostopoulou et al., 2008). However, Spencer and Slingo (2003) found that HadAM3 was able to accurately simulate large scale teleconnections due to the El Niño Southern Oscillation (ENSO). These are important to the UIB as variations in large-scale atmospheric circulation, linked to both the North Atlantic Oscillation and ENSO (Archer, 2003, 2004), are thought to be critical in influencing local variability in precipitation and temperature. Downscaling assumptions may also be invalidated if the relationship between circulation regimes and precipitation events are misrepresented (Ehret et al., 2012).

HadAM3P was forced using the 'high-emission' A2 SRES scenario (IPCC SRES, 2000) for 2071–2100 and compared with a control scenario (1961–1990). Recent emissions growth is in line with the SRES A2 scenario (Peters et al., 2013). These boundary conditions were used to drive PRECIS (Jones et al., 2004; HadRM3P) at a resolution of 0.44 decimal degrees (~50 km), over a limited domain which includes the UIB (hereafter PRECIS_AM3P). PRECIS was also run with boundary conditions from ERA-40, from 1957 to 2002 (hereafter PRECIS_ERA40).

3. Downscaling methodology

The downscaling methodology involves the generation of long "synthetic" weather time-series which allow robust assessment of the statistical distribution of possible future hydrological conditions. We use a pair of models which together function sequentially as a stochastic weather generator (Kilsby et al., 2007; Jones et al., 2009) to generate weather time-series at each of three stations in the UIB: Gilgit, Skardu and Astore.

3.1. Neyman–Scott Rectangular Pulses (NSRP) model

First, we generate a time-series of "synthetic rainfall" which simulates the statistical characteristics of the observed record. We use the single-site implementation of RainSim v3.1.1 which uses a Neyman–Scott Rectangular Pulses (NSRP) process to model rainfall accumulations (Burton et al., 2008). RainSim is used to provide simulations of the "control" climatology by fitting parameters to observed data to reproduce specified statistics of daily precipitation: mean, daily variance, proportion of dry days, skewness coefficient and the 1-day lagged autocorrelation. These statistics may then be perturbed using RCM-derived change factors for each calendar month and the model used to provide a simulation of future daily precipitation (see Kilsby et al., 2007 for further details).

3.2. Climatic Research Unit Daily Weather Generator (CRU-WG)

The synthetic precipitation time-series simulated by RainSim (Section 3.1) is then used to condition the Climatic Research Unit Daily Weather Generator (CRU-WG). This uses regression relationships between rainfall amount and temperature based on transitions between daily rainfall states (i.e. wet–wet, wet–dry, dry–wet, and dry–dry) as described in Kilsby et al. (2007). Whilst the CRU-WG is able to generate additional variables beyond air temperature (e.g. wind speed, potential evapotranspiration) these were not required in the present study (since historical observations were not available with which to calibrate the model).

The resultant set of self-consistent synthetic weather time-series (in this case for precipitation, minimum (T_{min}) and maximum (T_{max}) temperature) are then validated against the historical record by comparing their statistical properties to observations. Once the time-series have been validated, typically for the control period of a climate model experiment, a "perturbed" series may be generated using monthly change factors for the mean and daily variance of temperature (Jones et al., 2011).

3.3. Derivation of change factors

Perturbed series may be generated using change factors (CFs) which quantify relative changes in descriptive statistics between the simulated control climate and the projected future climate. Use of these CFs to perturb stochastically-generated synthetic time-series derived from the statistic properties of local observations provides a method of reducing or correcting bias which would be introduced if time-series of future climate conditions directly simulated by RCMs were utilised. Use of the synthetic time-series approach also permits greater exploration of the range of potential interannual and seasonal variability than would otherwise be offered by a simple perturbation of the 30-year observed time-series. The crucial caveat here is the assumption that biases are consistent between control and future simulations in a given RCM.

In this study, monthly CFs were calculated for mean rainfall, variance, proportion of dry days, skewness and lag-1 autocorrelation (Burton et al., 2008) and for temperature mean and variance and temperature range and variance (Kilsby et al., 2007; Jones et al., 2011). CFs for precipitation amounts, as well as for variance of all variables, are multiplicative whilst the CFs for temperature mean and range are additive. The constraining physical limit of dry-day probability (<1.0) and mathematical limits of autocorrelation (−1.0 to 1.0) must be recognised when applying calculated changes in these statistics (Burton et al., 2010). Full details of CF calculation and perturbation are provided in Kilsby et al. (2007) and Jones et al. (2009) and validation of the CF perturbation procedure is provided in Jones et al. (2011).

3.4. Definitions of selected indices

In a highly mountainous and glaciated areas such as the UIB, inputs of energy (air temperature) are equally important constraints to mass input (precipitation) in defining water resources availability and crop yields. Two indices, growing degree days (GD4) and growing season length (GSL), defined by the European Climate Assessment Project (ECA) (KNMI, 2012) were therefore selected to assess general thermal constraints on crop development (Table 1).

4. Validation of control climate

4.1. Precipitation

Synthetic precipitation time-series were generated for 100 30-year periods representing observed (control) climate conditions for 1961–1990 for the three UIB stations. Fig. 2a shows that monthly means of the 100 series very closely replicate the mean observations for each of the three stations. The root mean square error (RMSE) between the mean simulated and observed rainfall over 12 calendar months was 0.9 mm for Gilgit, 1.2 mm for Skardu and 1.8 mm for Astore. These values represent a simulation bias of only 4–8% of the annual mean daily rainfall at each station.

Fig. 2b–f illustrate the degree of agreement for each of the five statistics used by RainSim to fit the parameterisation of the NSRP process. Using Skardu as an example, the monthly means of the 100 simulations show good agreement with observations for mean daily rainfall (Fig. 2b) and daily rainfall variance (Fig. 2c). The results for proportion of dry-days (Fig. 2d), skewness (Fig. 2e) and 1-day lagged auto-correlation (Fig. 2f) also demonstrate reasonable agreement between observations and simulations. The skewness statistic shows the most repeated discrepancy with a consistent underestimation in the model, especially in late summer/autumn; while proportion dry-days and 1-day lagged autocorrelation show some discrepancy in March and June respectively. Results for the other two stations look similar to those for Skardu (not shown). Performance in simulation of the control climate for precipitation and wet-days is quantified in Table 2 which provides a range of biases in the monthly distribution (median, upper and lower quartiles) of these variables. Monthly RMSE is very small relative to annual totals while skill is roughly uniform across the distribution, i.e. performance for the quartiles is close to that for the median. Thus, for the first time this validates that RainSim can be used to successfully produce synthetic rainfall time-series in a semi-arid mountainous climate.

4.2. Air temperature

Corresponding synthetic temperature time-series were generated for 100 30-year periods representing observed (control) climate conditions for 1961–1990 for the three UIB stations using CRU-WG with the RainSim-simulated precipitation as input. The agreement between observed and simulated temperatures is demonstrated in Table 3 which shows minimum and maximum bias in monthly means for daily average temperature (T_{avg}) and diurnal temperature range (DTR) as well as absolute and relative RMSE for the first and last deciles as well as for the mean. For both T_{avg} and DTR there is a fractional positive bias in the synthetic time-series which is quite small when expressed as a fraction of the annual range (maximum of month minus minimum month) of T_{avg} (<2%) and annual mean DTR ($\leqslant$3.5%). This is also shown in Fig. 3 which demonstrates the annual cycle of maximum and minimum temperatures and DTR for observations and control simulations at Astore. Of arguably greater importance for the UIB than agreement of simulated and observed period means, is the agreement between the indicators of interannual variability, the first and last decile boundaries. To clarify, in Fig. 3 the values shown for WG output are mean of statistics the 100 30-year series, i.e. the ensemble mean for first and last deciles, rather than the first and last deciles of means within the ensemble. As Fig. 3 shows, for air temperature the performance of the WG in reproducing interannual variability rivals that achieved for period means. This skill is quantified in Table 3 which confirms that performance in simulation of the first and last deciles is nearly as good as for the mean.

In summary, the agreement between observed and simulated statistics for the "control climate" is good for all climate variables at all 3 UIB stations. This is satisfying given the large magnitude of annual cycles of precipitation and temperature in the UIB. Even more encouraging is the performance for interannual variability (quantified first and last deciles within each 30-year series). These

Table 1
Selected ECA indices for analysis.

Index	Description and definition (units)
GD4	Growing degree days (sum of $T_{avg} > 4$ °C) (°C)
GSL	Growing season length (days). GSL is calculated as the period length between the first occurrence when $T_{avg} > 5$ °C for six consecutive days until the first occurrence after 1 July when $T_{avg} < 5$ °C for six consecutive days

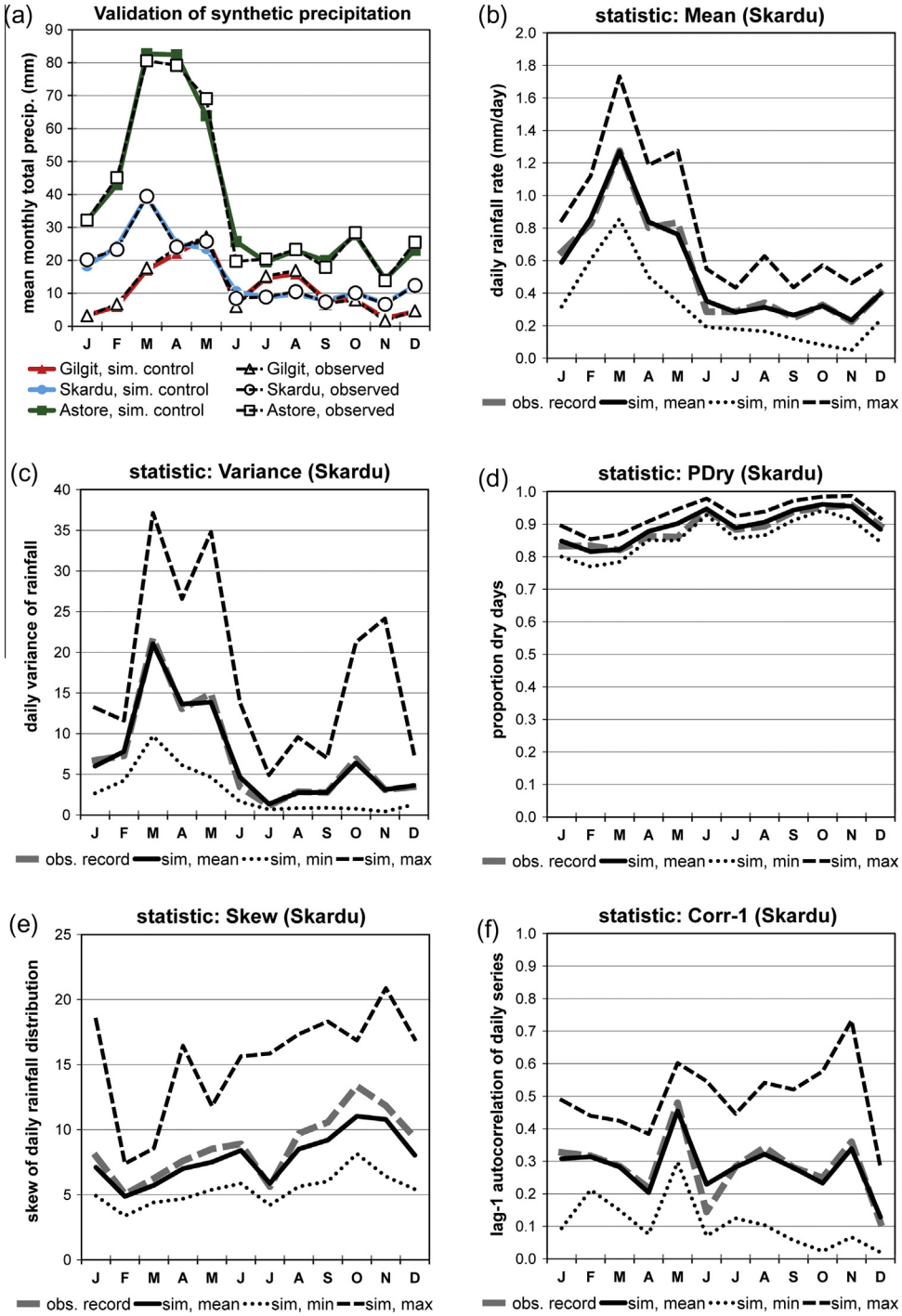

Fig. 2. Validation of synthetic "control climate" 100 30-year precipitation time-series generated by RainSim: (a) comparison of mean precipitation for the three selected stations (mean of 100 simulation means compared with observations); b–f: detail on the selected statistics for RainSim fitting using Skardu as an example; (b) mean daily rainfall rate; (c) variance of daily rainfall; (d) monthly proportion dry days; (e) skew of daily rainfall distribution; (f) 1-day (24 h) lagged autocorrelation. In panels b–f, the monthly value of the selected statistic from the observed recorded is compared to the corresponding results from the 100 30-year simulations: mean (sim, mean), minimum (sim, min) and maximum (sim, max) of the 100 simulations.

Table 2
Validation results of simulated control climate (1961–1990) precipitation variables: bias and RMSE.

Variable	Station	Statistic	Minimum monthly bias	Maximum monthly bias	Absolute RMSE	Observed representative value[a]	Relative RMSE
Monthly precipitation (mm)	Gilgit	Lower quartile	−2.7	+1.4	1.37	99.0	0.014
		Median	**−2.2**	**+3.6**	**1.33**	**128.9**	**0.011**
		Upper quartile	−5.9	+3.3	2.67	174.1	0.016
	Skardu	Lower quartile	−5.2	+5.7	2.82	145.5	0.020
		Median	**−3.9**	**+10.0**	**3.27**	**176.0**	**0.019**
		upper quartile	−10.4	+9.5	5.19	253.0	0.021
	Astore	Lower quartile	−3.9	+5.2	3.08	368.6	0.009
		Median	**−5.9**	**+7.1**	**3.72**	**442.9**	**0.009**
		Upper quartile	−17.4	+9.7	7.26	532.8	0.014
Monthly wet days	Gilgit	Lower quartile	−1.3	+0.3	0.72	32.2	0.023
		Median	**−2.8**	**+0.3**	**1.09**	**39.0**	**0.028**
		Upper quartile	−2.9	+0.6	1.44	44.5	0.033
	Skardu	Lower quartile	−2.0	+1.0	0.93	32.2	0.029
		Median	**−1.6**	**+0.5**	**0.75**	**42.0**	**0.018**
		Upper quartile	−0.8	+0.9	0.58	48.7	0.012
	Astore	Lower quartile	−1.8	+1.3	1.20	68.5	0.018
		Median	**−2.0**	**+1.1**	**1.24**	**80.0**	**0.016**
		Upper quartile	−2.5	+0.7	1.05	85.5	0.013

[a] Annual representative value for precipitation and wet days chosen as the respective annual totals.

results suggest that the weather generator methodology transfers well to a semi-arid environment.

5. Future climate scenarios

5.1. Assessment of climate model outputs

Before using GCM or RCM outputs for downscaling, it is first essential to consider whether the climate model adequately reproduces the regional climatology, or whether there are large biases. This can be challenging in mountainous regions where limited local observations, often located at relatively low elevations in valley settlements, are not representative of spatial mean conditions due to the dominant influence of elevation on air temperature and precipitation through environmental lapse rates and orographic enhancement. To overcome this we used a combination of reanalysis data to provide spatial means for absolute (scale-dependent) evaluation and local point observations for variables which are relatively independent of spatial scale and elevation. The common domain for spatial comparisons is shown in Fig. 1.

We evaluated RCM bias in both T_{avg} and DTR. Spatial means for T_{avg} were calculated using PRECIS_ERA40 for the common record period (1979–1990). Fig. 4A shows the excellent agreement between PRECIS_ERA40 and ERA-Interim. We then compared the PRECIS control run (1961–1990; PRECIS_AM3Pp) to the 1979–1990 averages from ERA-Interim and PRECIS_ERA40. We did not compare station values as they have very different absolute elevations than RCM values. Fig. 4A demonstrates that PRECIS_AM3Pp clearly shows an exacerbated annual cycle in comparison to the reanalysis products, with warm bias in summer (annual maxima) and cold bias in winter (annual minima). The same approach was used to evaluate bias in DTR, with additional direct comparison to station observations as only moderate elevation dependency in expected in DTR and this will decrease with elevation as lapse rates for T_{max} exceed those for T_{min}. Fig. 4B shows that, despite the relatively high elevation they represent, spatial mean DTR values for both PRECIS_AM3Pp and PRECIS_ERA40 exceed both observed values from local stations and those for ERA-Interim. However, as DTR from ERA-Interim is the difference between the warmest and coolest 6-hour means from the daily synoptic (00 h, 06 h, 12 h and 18 h UTC) analysis temperatures, DTR values would be expected to be muted in comparison to instantaneous maxima and minima for local observations or 5-min time step values from RCMs. Encouragingly, the PRECIS_AM3Pp annual DTR cycle has a similar shape to that of ERA-Interim and local meteorological stations, albeit with a positive bias of several degrees.

The net result of the air temperature bias assessment of PRECIS_ERA40 and PRECIS_AM3Pp is to provide mixed indications on RCM performance, highly dependent on the driving boundary conditions applied. These shortcomings reinforce the need for downscaling methods which as much as possible reduce transmission of RCM bias to downscaled climate data outputs.

Model simulation of total precipitation was first assessed by comparing spatial means (over the domain indicated in Fig. 1) from PRECIS_AM3Pp to PRECIS_ERA40 and ERA-Interim. Fig. 5A shows the agreement of the three data sources on the majority of annual precipitation occurring in the late winter and spring. Agreement is poorer in summer and autumn, with PRECIS_ERA40 showing a drier summer and wetter autumn and ERA-Interim indicating the reverse. PRECIS_AM3Pp, however, shows a consistent dry bias in relation to the other two data sets in early summer and mid-autumn.

The change factor approach applied in this study depends up on the validity of transferring the "proportionality" of the RCM-simulated response – from change in greenhouse gas forcing – to the

Table 3
Validation results of simulated control climate air temperature (1961–1990): bias and RMSE.

Variable	Station	Statistic	Minimum monthly bias (°C)	Maximum monthly bias (°C)	Absolute RMSE (°C)	Observed annual representative value[a] (°C)	Relative RMSE
Average daily temperature (T_{avg})	Gilgit	First decile	−1.2	0.6	0.50	23.5	0.022
		Mean	**0.0**	**+0.3**	**0.20**	**24.1**	**0.009**
		Last decile	−0.4	+1.8	0.61	24.7	0.025
	Skardu	First decile	−0.2	+0.7	0.40	27.3	0.015
		Mean	**0.0**	**+0.4**	**0.22**	**26.3**	**0.009**
		Last decile	−0.7	+0.4	0.33	25.5	0.013
	Astore	First decile	−0.8	+0.4	0.34	23.3	0.015
		Mean	**−0.1**	**+0.3**	**0.15**	**22.6**	**0.007**
		Last decile	−0.6	+0.5	0.40	22.2	0.019
Diurnal temperature range (DTR)	Gilgit	First decile	−0.5	+0.7	0.40	13.6	0.030
		Mean	**+0.1**	**+0.4**	**0.27**	**15.5**	**0.018**
		Last decile	−0.9	+0.5	0.47	17.7	0.027
	Skardu	First decile	+0.2	+1.3	0.71	11.0	0.065
		Mean	**+0.1**	**+0.5**	**0.27**	**12.9**	**0.021**
		Last decile	−1.7	0	0.76	15.1	0.051
	Astore	First decile	−0.7	+0.7	0.44	10.1	0.044
		Mean	**−0.5**	**+0.2**	**0.27**	**11.5**	**0.024**
		Last decile	−0.7	+0.4	0.37	12.7	0.030

[a] Annual representative value for T_{avg} chosen as the "annual range" (max monthly T_{avg} minus min monthly T_{avg}). Annual representative value for DTR was chosen as the annual mean DTR.

locally observed climatology in order to circumvent the biases inherent absolute model outputs (Diaz-Nieto and Wilby, 2005; Fowler et al., 2007). This approach is appropriate provided physical thresholds, e.g. available precipitable moisture, would not inhibit a proportional response relative to the observed climatology. A potential "second order" approach could adjust the calculated change factors as a function of the identified RCM control climate bias. With reference to Fig. 5A this could involve "amplifying" calculated change factors based on the ratio of reanalysis-forced (PRECIS_ERA40) precipitation divided by the GCM-driven (PRECIS_AM3Pp) precipitation. A visual appraisal of Fig. 5A suggests this would result in substantial increases to calculated change factors. A quantitative assessment of the implications of such an approach is beyond the scope of the present work.

A scale/elevation-independent metric was also identified for precipitation to allow direct comparison between RCM outputs and local observations. Mean monthly precipitation normalised by the corresponding mean annual precipitation yielded the mean monthly (fractional) contribution to annual precipitation. Fig. 5B shows good agreement for this statistic across the data sources, especially during the wettest months from February to May, apart from at Gilgit. Overall, this suggests that PRECIS simulations match well the observed seasonality of the control climate albeit whilst clearly not representing local-scale variability.

5.2. Regional climate model projections

Fig. 6 shows a comparison of statistics from the PRECIS control run (1961–1990; PRECIS_AM3Pp) and simulated future climate for the period 2071–2100 for the SRES A2 scenario (hereafter PRECIS_AM3Pf). Increases in T_{avg} are projected (Fig. 6A), with greater temperature increases in the summer months, perhaps due to excessive amplitude in the RCM annual temperature cycle. Fig. 6B shows little projected change in DTR, apart from a notable projected decrease in DTR from January to March.

Fig. 6C shows a substantial projected increase in precipitation in the wettest months of the year (February to May) under PRECIS_AM3Pf. In contrast, the only visible difference in monthly wet days (Fig. 6D) is a marginal reduction in August and September. These results seem consistent with an amplified hydrological cycle under increasing atmospheric GHG concentrations. Specifically, increased precipitation from February to May with a constant number of wet days and a relatively constant precipitation with decreasing wet days in August and September, points to increasing mean wet day intensity in all months.

5.3. Future scenarios using weather generator

To apply changes in temperature and precipitation projected by the RCM to the synthetic time-series generated by RainSim and CRU-WG, change factors were calculated as described in Section 3.3 to "perturb" the statistical descriptors of the control climate, and produce 100 sets of 30-year simulations of the perturbed climate conditions. CFs were calculated from the RCM grid cell overlying each station: Gilgit, Astore and Skardu. The monthly CFs for precipitation and temperature for each station are shown in Tables 4 and 5 respectively and reflect the changes presented in Fig. 6 as well as providing further information on changes in their statistical properties.

Fig. 7 shows the downscaled precipitation climatologies derived from the control and future (perturbed) synthetic time series compared to observations and as described by the median and lower and upper quartiles. The precipitation climatology projected by PRECIS_AM3Pf is relatively close to the observed historical (control) climate with the exception of increases in precipitation amounts during the wettest months of the year (February to

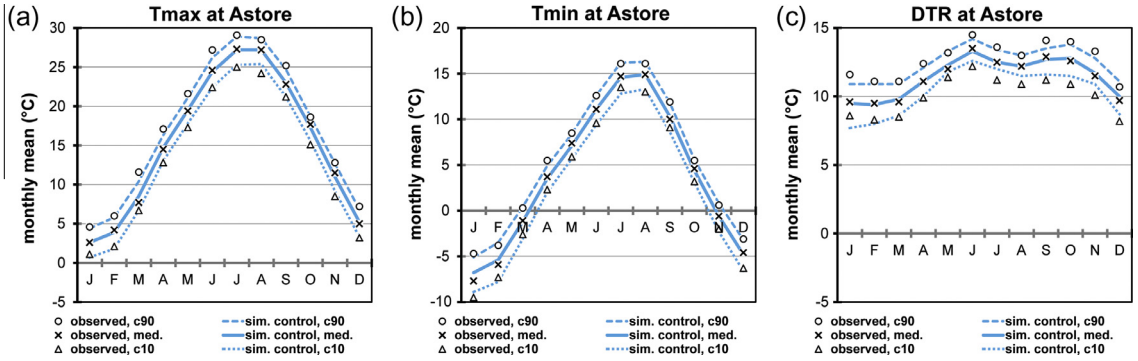

Fig. 3. Validation of synthetic control climate 100 30-year air temperature time-series generated by CRU WG: comparison of observations (obs) with simulated control climate (WG ctrl): (a) T_{max}; (b) T_{min}; and (c) DTR. In addition to period means, the interannual variability is assessed using the first (c10) and last (c90) deciles. All values are in °C.

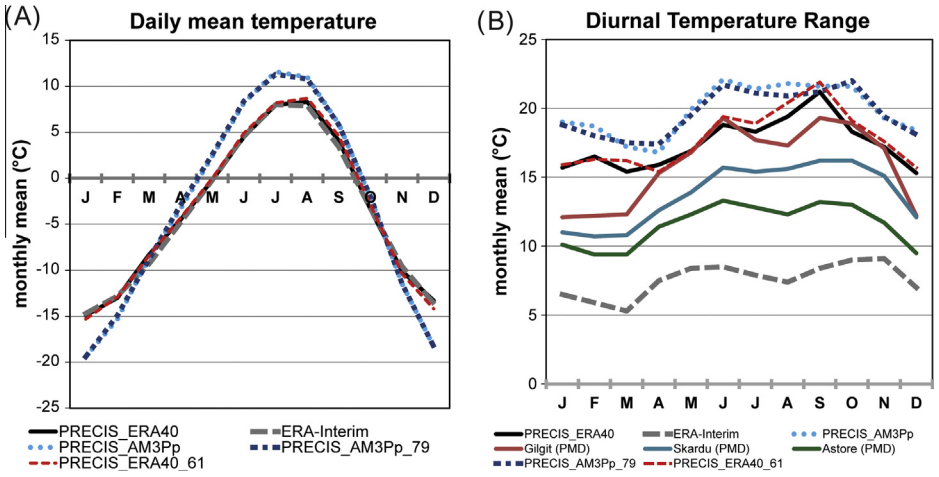

Fig. 4. Bias evaluation of RCM control climate air temperature outputs using available data sources (reanalysis and local observations) for spatial domain or observation points shown in Fig. 1: (A) annual cycle of daily mean temperature (T_{avg}); (B) annual cycle of diurnal temperature range (DTR) from both spatial means and (local) point observations. Note that it would not be expected that spatial means would match point observations in terms of magnitude.

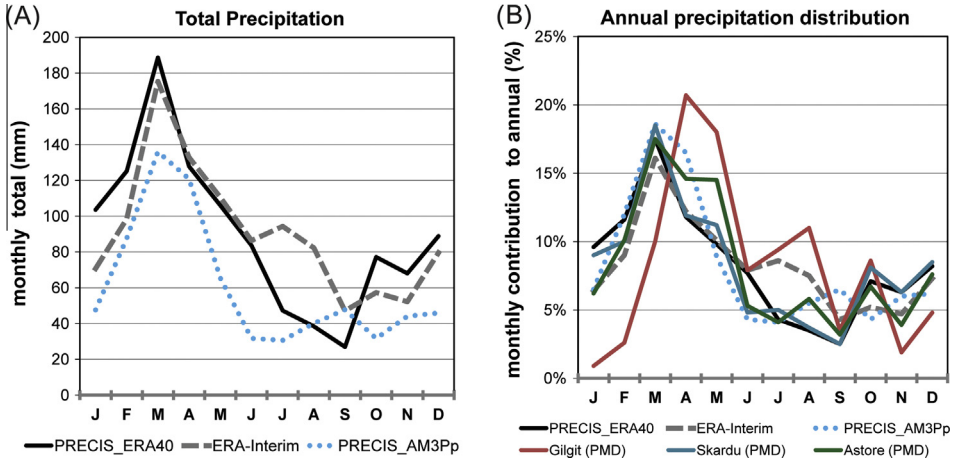

Fig. 5. Bias evaluation of RCM control climate outputs using available data sources (reanalysis and local observations): (A) spatially-averaged mean annual cycle of total precipitation; (B) mean annual cycles of mean monthly (fractional) contribution to annual total precipitation from both spatial means and (local) point observations.

May). For Gilgit this increase occurs only in the upper quartile boundary, while for Skardu increases occur in the median for March as well as in the upper quartile. Astore, in contrast, shows increases in the median from February to May and substantial increases in the upper quartile for the same months. Table 6 quantifies multiplicative seasonal changes between the perturbed and control simulated time-series across the statistical distribution (median, upper and lower quartiles) for precipitation amounts and wet day occurrence. Table 6 shows how in the wettest season, Spring (MAM), precipitation increases are amplified in the upper

quartile relative to the median and lower quartile. In contrast there is a relative "flattening" of the distribution of Summer (JJA) precipitation amounts with increases in the lower quartile and decreases in the upper quartile.

Table 7 quantifies additive seasonal changes between the perturbed and control simulated time-series across the statistical distribution (median, first and last deciles) for T_{avg} and DTR. Table 7 shows that differences across the distribution are relatively small compared to the changes between the perturbed and control simulated climates. The detail provided in Table 7 is a reminder that the weather generator approach integrates the influence of changes in precipitation occurrence – with implications for T_{avg} and DTR – along with the projected change factors for temperature mean and variance. Fig. 8 shows the projected near-surface air temperature climatology (median, first and last deciles) for Gilgit which provides a representative example amongst the 3 modelled stations. As expected based on the CFs used in CRU-WG, increases in T_{avg} are relatively uniform throughout the year, with marginally greater warming in summer months which is critical for snow and ice melt processes. To put into context the magnitude of projected warming, the simulated future first decile (Fig. 8: sim. perturb., c10) of T_{avg} is warmer in every month than the control climate last decile (sim. control, c90). Projected changes in DTR are however relatively limited with notable decreases in January to March and marginal decreases from October to December. This suggests that the UIB will continue to experience large diurnal temperature cycles under global warming. This is important not only for local hydrology, where night-time refreezing can interrupt the generation and transport of glacial meltwater contributions to runoff, but also for local agriculture where frost events could jeopardise crop yields.

5.4. Key indices of future climate

While the statistical descriptors of climate variables under future conditions provide an initial picture of possible impacts on regional water resources and local food security, further insight can be gained by examining selected climate indices (see Table 1).

While the local long-record UIB meteorological stations are located at relatively low (1460 m to 2394 m asl) elevations on valley floors the vast majority of catchment area is found high above these levels (Forsythe et al., 2012b). Nonetheless, GD4 and GSL (Table 1) are useful as indicators of energy constraints for meltwater generation not only at the base elevation of the meteorological stations, but also at higher elevations by using lapse rates identified in previous analyses. Hashmi and Shafiullah (2003) identified the upper limits of the single cropping zone and high level pasture or forest land respectively as 3000 m asl and 4500 m asl in the UIB. As described by Forsythe et al. (2012a,b), examination of the hypsometry of the UIB shows that slightly less than 20% of UIB surface area is located below 3000 m asl. For these reasons it was decided to extrapolate values for both GD4 and GSL for elevations of 3000 m and 4500 m asl. Air temperatures were calculated by

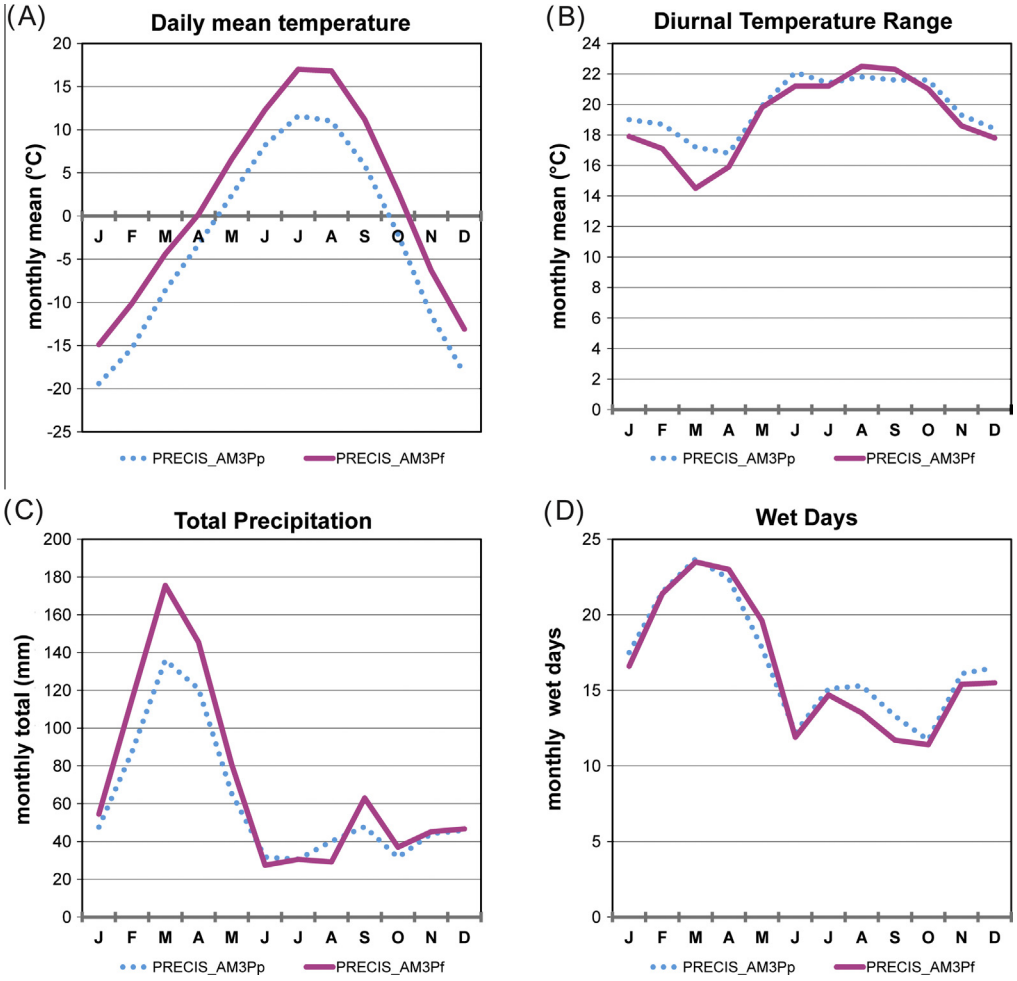

Fig. 6. Comparison of projected future climate (PRECIS_AMP3f) to simulated control climate (PRECIS_AM3Pp) for key climate variables: (A) T_{avg}; (B) DTR; (C) total precipitation; (D) monthly wet days. Values shown are spatial means over the domain indicated in Fig. 1.

Table 4
CFs for precipitation statistics at Gilgit, Skardu and Astore.

Statistic	Station	January	February	March	April	May	June	July	August	September	October	November	December
Mean	Gilgit	1.23	1.27	1.24	1.19	1.08	0.72	1.04	0.64	1.48	1.27	1.08	1.05
	Skardu	1.15	1.30	1.44	1.37	1.40	1.01	0.96	0.73	1.52	1.17	1.23	1.06
	Astore	1.18	1.34	1.34	1.35	1.42	0.94	1.01	0.73	1.48	1.25	1.03	0.99
Variance	Gilgit	1.90	2.27	1.53	1.63	1.62	0.38	0.63	0.40	3.12	2.36	1.40	1.20
	Skardu	2.27	2.41	2.29	2.12	3.70	0.95	1.22	0.41	3.68	1.07	2.54	1.20
	Astore	1.71	2.20	1.89	2.09	2.92	0.61	1.07	0.39	2.47	1.47	1.41	1.07
Proportion dry days	Gilgit	0.99	1.01	1.06	1.10	1.11	1.03	1.02	1.11	1.02	1.01	0.96	0.96
	Skardu	1.03	0.97	1.05	1.05	1.07	0.97	0.94	0.98	0.97	0.99	0.96	0.99
	Astore	1.04	1.13	1.15	1.21	1.22	1.09	1.08	1.10	1.14	1.01	0.97	1.07
Skew	Gilgit	1.21	1.22	0.84	1.20	1.44	1.06	0.62	1.15	1.54	1.35	1.17	0.90
	Skardu	1.79	1.39	0.99	1.30	3.14	1.11	1.74	0.61	1.26	0.98	1.89	0.69
	Astore	1.05	1.16	0.98	1.32	1.98	1.07	1.31	0.93	1.13	1.14	1.29	0.79
Lag-1 auto-correlation	Gilgit	1.12	1.15	0.23	1.18	0.92	−0.26	−0.23	−0.94	0.68	0.98	−0.64	−0.63
	Skardu	1.15	1.02	0.74	0.77	0.98	−0.44	0.01	0.87	0.18	0.61	1.45	−0.88
	Astore	1.23	1.31	0.82	1.01	1.00	0.37	−1.16	0.44	0.67	0.77	1.15	0.36

Table 5
CFs for air temperature statistics at Gilgit, Skardu and Astore.

Variable	Statistic	Station	January	February	March	April	May	June	July	August	September	October	November	December
T_{avg}	Mean	Gilgit	4.8	4.9	5.7	3.1	4.7	4.5	6.1	6.1	5.4	4.5	5.5	5.7
		Skardu	5.3	5.6	4.8	2.9	3.8	3.8	5.6	5.9	5.4	4.9	5.3	5.7
		Astore	4.1	4.6	4.6	4.3	4.0	4.1	5.8	6.5	6.1	5.0	5.2	4.9
	Variance	Gilgit	1.719	1.013	1.694	1.44	1.983	0.914	0.821	0.622	3.348	2.719	1.015	0.569
		Skardu	0.793	0.881	0.71	1.669	0.862	1.509	1.365	0.731	1.944	1.994	0.911	0.609
		Astore	1.434	0.619	2.74	0.498	1.568	1.028	1.181	0.442	1.772	1.069	1.146	1.000
DTR	Mean	Gilgit	−1.7	−2.4	−2.6	0.9	0.9	−0.3	−0.2	0.2	−0.4	−1.0	−1.4	−1.4
		Skardu	−1.1	−1.3	−2.1	−1.8	−1.5	−1.6	−1	−0.5	−0.9	−1.1	−0.9	−1.0
		Astore	−1.2	−1.7	−2.5	0.3	−0.2	−1.9	−0.6	0.5	0.2	−0.2	−0.8	−0.6
	Variance	Gilgit	1.121	1.491	1.305	1.351	0.755	0.541	0.587	0.450	0.926	0.908	1.771	1.320
		Skardu	0.570	1.238	0.910	1.314	0.953	0.925	0.865	0.545	1.13	0.888	0.503	0.614
		Astore	0.541	0.745	1.733	1.362	0.539	0.654	0.679	0.603	0.794	0.672	1.444	0.930

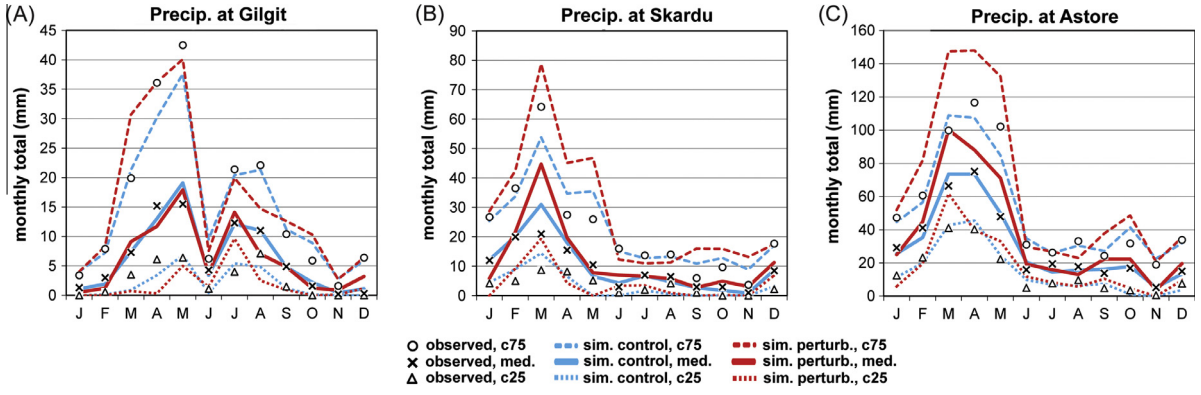

Fig. 7. Comparison of statistics between observations and simulated climate time-series for precipitation for: (A) Gilgit; (B) Skardu; (C) Astore. Blue lines show simulated control climate ("sim. control"). Red lines show simulated future climate ("sim. perturb."). Black symbols indicate the statistics of the observed record ("observed"). Values are shown for the median (med.), lower quartile (c25) and upper quartile (c75) boundaries. The values for "sim. control" and "sim. perturb." are calculated as the mean of the 100 simulations for the statistic (med, c25, c75) within the 30-year time-series. (For interpretation of the references to colour in this figure legend, the reader is referred to the web version of this article.)

applying a lapse rate of −7.0 °C per 1000 m to simulated T_{avg} at the modelled stations.

Calculation of annual total GD4 and GSL at 3000 m and 4500 m asl as shown in Fig. 9 reveals the influence of temperature thresholds in distorting incremental temperature changes under future climate, with GD4 increasing by a factor of roughly 1.6 at 3000 m asl but by 3–4 at 4500 m asl. The difference in changes to GSL is even more striking. At 3000 m asl the extension of season length is between 30 and 50 days under future climate, increasing by a factor of 1.3. This may be enough to allow a greater choice of crops or more reliable attainment of plant maturity, but is still an incremental rather than order of magnitude increase. The projected changes at 4500 m asl are particularly striking as at this elevation crop growth is marginal under current climate conditions (median GSL values at or near to 0 days). Under the future climate, however, median GSL values reach or exceed 10 weeks (70 days). Nevertheless, first decile (c10) GSL values are still less than 20 days, showing that even with strong warming, at this elevation conditions remain

Table 6
Simulated future air temperature: changes in distribution of T_{avg} and DTR, perturbed synthetic time-series with respect to synthetic control climate.

Variable	Station	Statistic	Average seasonal multiplicative change (dimensionless)			
			Winter (DJF)	Spring (MAM)	Summer (JJA)	Autumn (SON)
Seasonal precipitation (mm)	Gilgit	Lower quartile	12.000	0.540	1.273	0.769
		Median	**1.195**	**0.979**	**0.935**	**0.932**
		Upper quartile	1.093	1.200	0.822	1.117
	Skardu	Lower quartile	0.964	1.128	3.391	[a]
		Median	**0.943**	**1.298**	**1.227**	**2.000**
		Upper quartile	1.162	1.375	0.841	1.383
	Astore	Lower quartile	0.997	1.192	1.126	1.747
		Median	**1.203**	**1.316**	**0.952**	**1.225**
		Upper quartile	1.269	1.421	0.872	1.173
Monthly wet days	Gilgit	Lower quartile	3.000	0.531	2.254	0.937
		Median	**1.419**	**0.791**	**1.509**	**0.851**
		Upper quartile	1.163	0.870	1.256	0.788
	Skardu	Lower quartile	1.093	0.745	3.684	4.000
		Median	**1.015**	**0.883**	**1.761**	**1.461**
		Upper quartile	0.990	0.868	1.357	1.416
	Astore	Lower quartile	0.436	0.702	1.325	0.148
		Median	**0.740**	**0.854**	**1.187**	**0.747**
		Upper quartile	0.877	0.923	1.137	0.860

[a] Simulated Skardu control climate had near-zero (<0.05 mm) lower quartile Autumn precipitation, hence near infinite multiplicative change (divide by zero).

highly sensitive to minor fluctuations inherent from intrinsic interannual variability.

While the GD4 and GSL indices are primarily targeted at crop productivity constraints they also serve as indicators respectively of available energy for meltwater runoff generation and potential glacial melt season duration. The "degree day method" (Singh et al., 2000) is a common approach for calculation of snowmelt runoff. This method is analogous to the definition of GD4 with the difference that the reference threshold is generally 0 °C rather than 4 °C. As such GD4 provides a more conservative indicator than a "pure" degree day calculation. Furthermore, work by Forsythe et al. (2012a,b) has shown that river discharge from the highly glacierised UIB tributary basin Hunza is highly correlated to the fraction of catchment experiencing "continuous melt" conditions, i.e. where $T_{min} > 0$ °C. As such the GSL indicator dependent on sustained conditions with $T_{avg} > 5$ °C may serve as a proportional indicator of the potential duration of intense glacial melt. Previous work by Archer (2004), confirmed by Forsythe et al. (2012a,b), has shown that the T_{min} freezing (0 °C) isotherm in the UIB is near to or above 4500 m asl from June through September. Thus calculation of the GD4 and GSL indices at this elevation are relevant to hydrological studies of the basin. The substantial increases found for these indices suggest the potential for profound changes to the hydrology in these elevation zones of UIB tributary catchments. Such changes could include greater fraction of precipitation falling as rain (rather than snow), rapid ablation of seasonal snowpack, and largely negative glacial mass balances leading to eventual transformation from glacial to nival hydrological regimes in currently glaciated areas.

6. Discussion and conclusions

6.1. Consideration of alternate change trajectory for air temperature

The relative changes (increases) in temperature, represented by change factors, from PRECIS_AM3Pf and PRECIS_AM3Pp are of similar magnitude to those reported for the region by Ozturk et al. (2012) although somewhat larger than those found by Mathison et al. (2014) for the adjacent Ganges–Brahmaputra basin. These spatially and seasonally homogenous projected increases in air temperature are, however, in stark contrast to the observed seasonally asymmetrical trends, rapid warming in Winter and Spring but moderate cooling in Summer, in recent decades for local point observations (Fowler and Archer, 2006), ERA-Interim and PRECIS_ERA40 (Fig. 10). Comparing panels A (1961–1990) and B (1979–2007) of Fig. 10, shows that this finding is consistent among the data sources and is apparent over both timeframes. There is consistency between the two time periods in strong warming in late autumn and late spring contrasted by cooling in summer and cooling or stationary temperatures in early autumn.

The agreement between the trend estimates from local observations and those from the reanalysis and RCM data sources is quantified in Table 8 which shows Pearson's correlation values of the 12 calendar month series of trend estimates along with their corresponding statistical significance based on a 2-tailed Student's *T*-test. For the 1961–1990 reference period correlations for both Gilgit and Skardu to the gridded data sources are significant at the 95% level ($p < 0.05$). For the more recent 1979–2007 period, correlations of all 3 stations with ERA-Interim are significant at the 99% level ($p < 0.01$).

To explore the potential impacts of continued summer cooling as observed, in contrast to the strong warming indicated by RCM projections, modifications were made to the CFs for mean T_{avg} by replacing the time slice-derived values as follows: July and August = −3.0 °C, June and September = 0.0 °C, all other months

Table 7
Simulated future air temperature: changes in distribution of T_{avg} and DTR, perturbed synthetic time-series with respect to synthetic control climate.

Variable	Station	Statistic	Average seasonal additive change (°C)			
			DJF	MAM	JJA	SON
Average daily temperature (T_{avg})	Gilgit	First decile	+5.0	+4.0	+5.6	+4.4
		Median	**+5.0**	**+4.5**	**+5.4**	**+5.1**
		Last decile	+4.9	+4.9	+5.2	+5.6
	Skardu	First decile	+5.7	+3.8	+4.9	+4.9
		Median	**+5.4**	**+3.9**	**+4.9**	**+5.1**
		Last decile	+5.2	+3.9	+5.0	+5.4
	Astore	First decile	+4.3	+4.0	+5.6	+5.1
		Median	**+4.4**	**+4.5**	**+5.4**	**+5.4**
		Last decile	+4.4	+4.8	+5.2	+5.6
Diurnal temperature range (DTR)	Gilgit	First decile	−2.0	−0.2	+0.3	−1.2
		Median	**−1.8**	**−0.1**	**−0.1**	**−0.8**
		Last decile	−1.6	0	−0.7	−0.6
	Skardu	First decile	−1.0	−1.8	−0.9	−1.0
		Median	**−1.1**	**−1.7**	**−1.1**	**−0.8**
		Last decile	−1.3	−1.7	−1.2	−1.2
	Astore	First decile	−0.9	−0.7	−0.4	−0.2
		Median	**−1.1**	**−0.6**	**−0.6**	**−0.3**
		Last decile	−1.2	−0.5	−0.8	−0.3

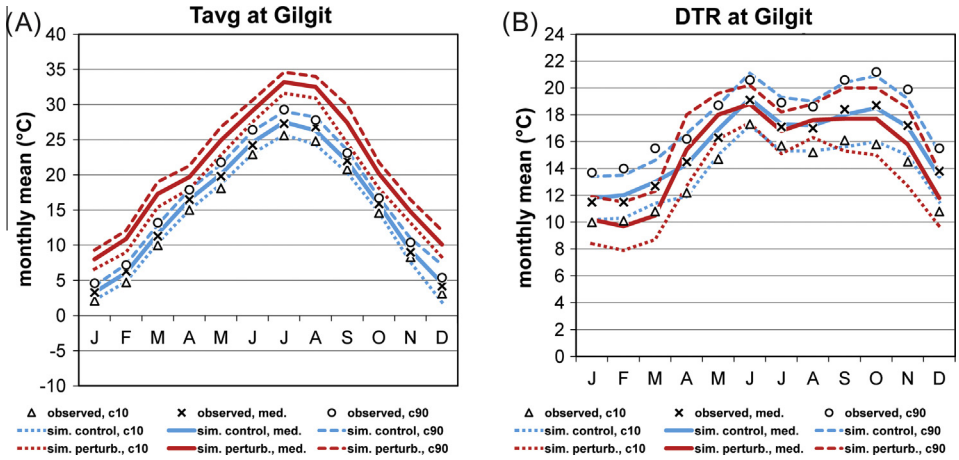

Fig. 8. Comparison of statistics between observations and simulated climate time-series for air temperature at Gilgit: (A) T_{avg}; (B) DTR. Blue lines show simulated control climate, 1961-1990 ("sim. control"). Red lines show simulated future climate, 2070–2100 ("sim. perturb."). Black symbols indicate the statistics of the observed record ("observed"). Values are shown for the median (med), first decile (c10) and last decile (c90) boundaries. The values for "sim. control" and "sim. perturb." are calculated as the mean of the 100 simulations for the statistic (med, c10, c90) within the 30-year time-series. (For interpretation of the references to colour in this figure legend, the reader is referred to the web version of this article.)

as previously determined. These values were derived from Fig. 10 (0.03 °C/year cooling in summer). The extrapolation procedure for higher elevations was then repeated. This approach thus maintains projected strong warming through late spring (beginning of growing/melting season) and from mid-autumn (end of growing season).

The results of this exercise, shown in Table 9, further illustrate how (physical) temperature thresholds can amplify the relative impacts of potential climate change. At 3000 m asl, for GD4, summer cooling is compensated by spring and autumn warming as the "extrapolated trends" estimate are still approximately 15% greater than in the control climate, even if far less than the 50–70% increases in the estimates based on RCM projections. For GSL at 3000 m asl temperatures are warm enough that the controlling months are in the spring and autumn. Thus as the projected warming in those months was retained, and because the hypothesised summer cooling was not severe enough to interrupt mid-season growing conditions, "extrapolated trends" 3000 m GSL estimates are effectively identical to those from RCM projections, showing increases of roughly 30%.

At 4500 m asl, however, temperatures in spring and autumn do not reach growing condition threshold levels (even after projected warming), and thus focus is squarely on the peak summer months. GD4 estimates from "extrapolated trends" show a 20% to 40% decrease in comparison to the control climate whereas the RCM projections show increases of 150–300% (factors of 2.5–4). GSL estimates from "extrapolated trends" are effectively identical to the control climate values as the perturbed variance results in some years still reaching threshold levels despite the mean cooling. Thus under both the control climate and "extrapolated trends" conditions satisfaction of the GSL threshold criteria remains infrequent. This is in stark contrast to the RCM projections where 9 out of 10 years (first decile) have GSL values of at least one week (7 days), with median values of 11 weeks or more.

As explained in Section 5.4, the GD4 and GSL indices can be seen as indicators of the energy available to drive the melting of glacial ice and seasonal snowpack which generates the runoff from which flows in the Upper Indus and its tributaries are composed. Recent studies (Gardelle et al., 2012; Jacob et al., 2012) have identified apparent widespread increases in the volume and mass of glaciers

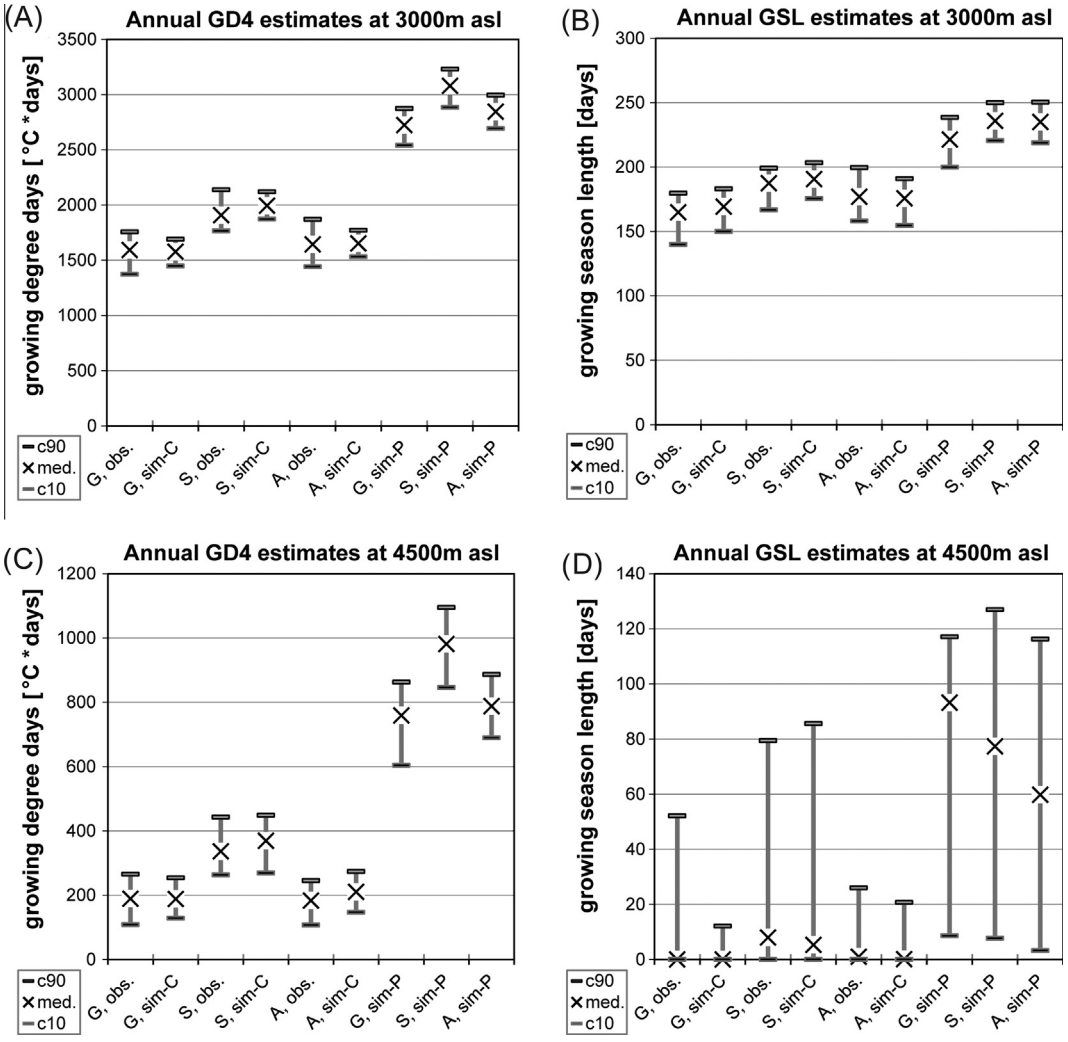

Fig. 9. Indicators of thermal constraints on crop development and meltwater runoff generation, comparison between estimates from synthetic time series and from observations at modelled stations: (A) GD4 at 3000 m asl; (B) GSL at 3000 m asl; (C) GD4 at 4500 m asl; and (D) GSL at 4500 m asl. Values are shown for the median, first decile (c10) and last decile (c90) boundaries. In the horizontal axes labels the initial letters indicate stations: *G* = Gilgit; *S* = Skardu; *A* = Astore. The second portion of the horizontal axes labels indicates data source: "obs." = observed record; "sim-C" = simulated control climate; "sim-P" = simulated perturbed climate. The values for "sim-C" and "sim-P." are calculated as the mean of the 100 simulations for the statistic (med., c10, c90) within the 30-year time-series.

in the Upper Indus. One potential explanation is a reduction in the available energy, observed in summer air temperature cooling, to drive annual melting at high elevations. Sharif et al. (2013) found corresponding reductions in runoff from glacial catchments. Thus any continuation of summer air temperature cooling could pose a substantial risk, through insufficient energy inputs to transform glacial ice and seasonal snow to runoff, to populations dependent on water resources from the Upper Indus. The real conundrum here is whether this cooling is a local or regional circulation effect and whether it will continue or even become accentuated under global warming, as GCMs cannot reproduce this phenomenon.

6.2. Summary and conclusions

This study coupled the NSRP rainfall model (RainSim v3.1.1) to the CRU Daily Weather Generator to generate long synthetic time-series of precipitation and temperature for 'present' and future time periods for three UIB meteorological stations. This is the first application of the RainSim/CRU-WG coupled tool to a climate domain outside Europe and the first to a semi-arid mountainous climate. Prior to their use, air temperature and precipitation climatologies from the control RCM simulations, PRECIS_ERA40 and PRECIS_AM3Pp, were compared to meteorological reanalysis and local observations to assess bias and confirm that the key features of annual cycles were adequately reproduced. Differences between the control (1961–1990) and future (2071–2100) regional climate model (RCM) time-slice experiment were then used to provide change factors which could be applied within the weather generator to produce perturbed 'future' weather time-series. The results showed projections of year-round increases in precipitation (maximum seasonal mean change: +27%, annual mean change: +18%) with increased intensity in the wettest months (February, March and April) as well as year-round increases in mean temperature (domain annual average +4.8 °C). The uniformity of projected temperature increases is in stark contrast to asymmetrical recent trends in observations.

In addition, selected ECA indices were calculated to assess climatic constraints, as inputs of energy (temperature), on the productivity of natural resource-dependent systems. Thermal constraints on crop growth were assessed using standard indices of energy inputs (growing degree days, GD4) and growing season length (GSL). Although these indicators were designed in terms of agricultural systems, given the high-elevation context of the UIB they can also be seen as proxies for thermal inputs to melting

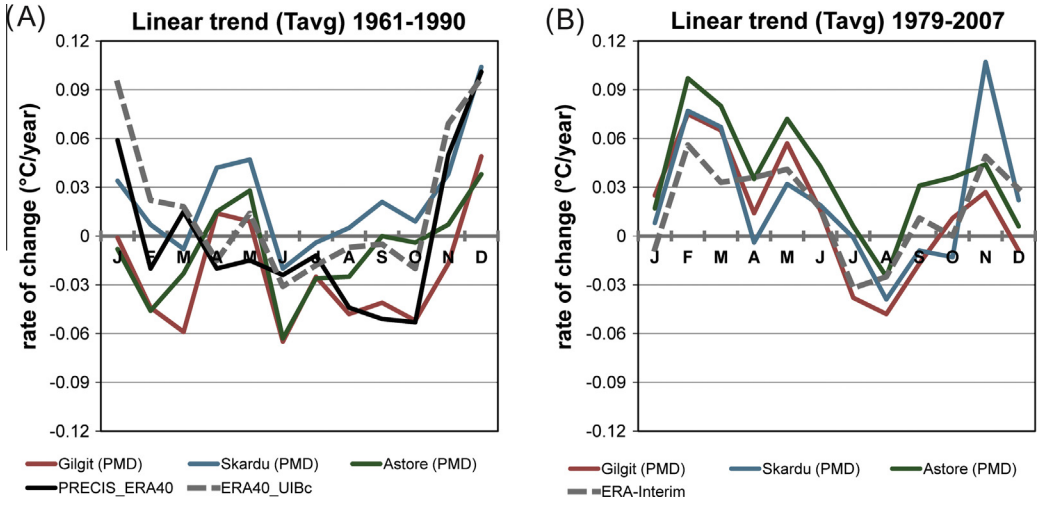

Fig. 10. Seasonally asymmetrical temperature trends (T_{avg}) from multiple data sources for two time periods: (A) 1961–1990; and (B) 1979–2007. Data sources include: local observations (PMD), ERA-40 (ERA40_UIBc), ERA-Interim and PRECIS_ERA40. Values are in units of (°C year^{-1}).

Table 8
Correlations and their significance between trend estimates from local observations and reanalysis and RCM data sources.

Station	T_{avg} trends: 1961–1990				T_{avg} trends: 1979–2007	
	PRECIS_ERA40		ERA40		ERA-Interim	
	Pearson's r	Significance p	Pearson's r	Significance p	Pearson's r	Significance p
Gilgit (PMD)	0.611	0.035	0.655	0.021	0.777	0.003
Skardu (PMD)	0.691	0.013	0.663	0.019	0.762	0.004
Astore (PMD)	0.467	0.126	0.422	0.172	0.773	0.004

Table 9
Comparison of ECA thermal indicators under contrasting trajectories for air temperature change in the UIB.

Index	Elev.	Source station	RCM projections			Control climate			Extrapolated trends		
			c10	med.	c90	c10	med.	c90	c10	med.	c90
GD4	3000 m asl	Gilgit	2541.2	**2724.4**	2873.1	1448.5	**1576.2**	1689.9	1694.6	**1869.8**	2016.0
		Skardu	2884.7	**3079.7**	3231.6	1872.4	**1994.1**	2119.9	2098.3	**2264.4**	2424.6
		Astore	2797.3	**2946.5**	3080.3	1605.5	**1723.7**	1830.6	1955.4	**2074.0**	2207.5
	4500 m asl	Gilgit	604.4	**759.2**	862.8	128.6	**188.4**	254.2	108.2	**152.9**	211.9
		Skardu	846.1	**981.3**	1095.3	269.4	**369.1**	448.7	207.8	**299.1**	383.1
		Astore	715.5	**827.6**	910.7	153.4	**204.4**	259.2	93.6	**139.1**	188.4
GSL	3000 m asl	Gilgit	199.9	**221.4**	238.6	150.0	**169.3**	183.2	176.1	**218.6**	237.7
		Skardu	220.6	**235.9**	250.0	175.6	**190.8**	203.3	213.0	**234.7**	249.0
		Astore	222.0	**238.8**	255.4	163.4	**181.3**	196.9	220.5	**238.4**	254.7
	4500 m asl	Gilgit	8.6	**93.2**	117.1	0	**0**	12.1	0	**2.3**	11.5
		Skardu	7.7	**77.4**	127	0	**5.3**	85.6	0.5	**8.1**	39.5
		Astore	7.2	**94.4**	124.1	0	**0.1**	23.5	0	**3.3**	12.9

of glacial ice and seasonal snowpack. In addition to the GD4 and GSL estimates from perturbed and control climate time-series, a further potential climate "trajectory" based on the continuation of recent observed summer cooling was assessed.

The implications of these divergent trajectories in terms of available energy to drive meltwater runoff generation and crop productivity were compared amongst the three UIB stations for two representative elevations, 3000 m and 4500 m asl, after extrapolation using lapse rates. This comparison revealed that sensitivity to incremental temperature shifts is exacerbated at higher elevations due to the narrowing gap between seasonal temperatures and key thresholds. The large increases in temperature and hence available energy under the RCM projections yield substantial increases in local GD4 and GSL values. From a regional viewpoint there is a risk that increased thermal inputs could potentially more than offset projected precipitation increases through increased evapotranspiration (Wetherald and Manabe, 2002). In contrast, projected precipitation increases under the "extrapolated trends" trajectory might not be translated into increased runoff and crop growth if the projected summer cooling results in insufficient energy to transform the added mass input into meltwater runoff. Severe cooling could result in decreasing river flows. Thus both potential trajectories represent important, albeit differentiated, risks.

There are a number of caveats to this study. Uncertainty in climate projections stem from a number of factors. These include: the unknown trajectory of anthropogenic greenhouse gas emissions; climate modelling uncertainties, including resolution, parameterisations, structure; and for RCMs, boundary conditions, and the assumption of stability of model biases in a changing climate. For

these reasons, it is recommended that in hydrological impact studies that wherever possible use should be made of scenarios from multiple climate model experiments often referred to as 'ensembles' (Fowler et al., 2007). Here we use only one pair of simulations, control and future, from a single RCM driven by one GCM. For this reason, the results presented here are intended to provide a demonstration of the applicability of this downscaling methodology for use in semi-arid environments rather than an exhaustive exploration of uncertainty in climate projections for the UIB. In furthering the present work, it would be advantageous to draw on an "ensemble" of RCM simulations (such as the soon to be available CORDEX experiments), as now widely adopted in climate change impact assessments (e.g. van Vliet et al., 2012), to better capture the range of uncertainty identified by available GCM simulations.

Finally, current interannual variability is comparable to or exceeds the projected relative changes in mean precipitation in the UIB. Thus changes in interannual variability of key climate inputs may be of equal or greater importance than incremental changes in mean conditions in determining future water availability for irrigated agriculture. This demonstrates the importance of climate change impact assessment methodologies that fully investigate interannual variability for robust evaluation of future risks to regions such as the UIB. Stochastically generated synthetic time-series which can used as input for probabilistic modelling are foremost examples of such methodologies. The successful application of the CRU WG to the semi-arid climate of the UIB represents an important step forward in expanding the geographic application of this approach. This opens the way for more sophisticated climate change impact assessments in mountainous and semi-arid regions which can provide more skilled evaluations than can be delivered by simpler downscaling methods such as the "delta change" approach.

Acknowledgments

This study was made possible by financial support from the Leverhulme Trust via a Philip Leverhulme Prize (2011) awarded to Prof. Fowler. RCM outputs were provided by the Global Change Impacts Studies Centre (GCISC). Local meteorological data was acquired from the Pakistan Meteorological Department (PMD). Additional financial support during the developmental stages of this work was provided by the British Council (PMI2 and INSPIRE Grants), the UK Natural Environment Research Council (NERC) as a Postdoctoral Fellowship award NE/D009588/1 (2006–2010) to Prof. Fowler, and a US National Science Foundation (NSF) Graduate Research Fellowship award to Dr. Forsythe (2006–2010).

References

Akhtar, M., Ahmad, N., Booij, M.J., 2008. The impact of climate change on the water resource of Hindukush–Karakorum–Himalaya region under different glacier coverage scenarios. J. Hydrol. 355 (1–4), 148–163. http://dx.doi.org/10.1016/j.jhydrol.2008.03.015.

Anagnostopoulou, C., Tolika, K., Maheras, P., Kutiel, H., Flocas, H., 2008. Performance of the general circulation HadAM3P model in simulating circulation types over the Mediterranean region. Int. J. Climatol. 28 (2), 185–203. http://dx.doi.org/10.1002/joc.1521.

Archer, D.R., 2003. Contrasting hydrological regimes in the Indus Basin. J. Hydrol. 274 (1–4), 198–210. http://dx.doi.org/10.1016/S0022-1694(02)00414-6.

Archer, D.R., 2004. Hydrological implications of spatial and altitudinal variation in temperature in the Upper Indus Basin. Nord. Hydrol. 35 (3), 209–222.

Archer, D.R., Fowler, H.J., 2008. Using meteorological data to forecast seasonal runoff on the River Jhelum, Pakistan. J. Hydrol. 361 (1-2), 10–23. http://dx.doi.org/10.1016/j.jhydrol.2008.07.017.

Archer, D.R, Forsythe, N., Fowler, H.J., Shah, S.M., 2010. Sustainability of water resources management in the Indus Basin under changing climatic and socio economic conditions. Hydrol. Earth Syst. Sci. 14, 1669–1680. http://dx.doi.org/10.5194/hess-14-1669-2010.

Barnett, T.P., Adam, J.C., Lettenmaier, D.P., 2005. Potential impacts of a warming climate on water availability in snow-dominated regions. Nature 438, 303–309. http://dx.doi.org/10.1038/nature04141.

Berrisford, P., Kallberg, P., Kobayashi, S., Dee, D., Uppala, S., Simmons, A.J., Poli, P., Sato, H., 2011. Atmospheric conservation properties in ERA-Interim. Quart. J. Roy. Meteorol. Soc. 137 (659), 1381–1399. http://dx.doi.org/10.1002/qj.864.

Betts, A.K., Kohler, M., Zhang, Y., 2009. Comparison of river basin hydrometeorology in ERA-Interim and ERA-40 reanalyses with observations. J. Geophys. Res. 114 (D2), D02101. http://dx.doi.org/10.1029/2008JD010761.

Blenkinsop, S., Harpham, C., Burton, A., Goderniaux, P., Brouyère, S., Fowler, H.J., 2013. Downscaling transient climate change with a stochastic weather generator for the Geer catchment. Belgium. Climate Res. 57 (2), 95–109. http://dx.doi.org/10.3354/cr01170.

Bocchiola, D., Diolaiuti, G., Soncini, A., Mihalcea, C., D'Agata, C., Mayer, C., Lambrecht, A., Rosso, R., Smiraglia, C., 2011. Prediction of future hydrological regimes in poorly gauged high altitude basins: the case study of the upper Indus, Pakistan. Hydrol. Earth Syst. Sci. 15 (7), 2059–2075. http://dx.doi.org/10.5194/hess-15-2059-2011.

Burton, A., Kilsby, C.G., Fowler, H.J., Cowpertwait, P.S.P., O'Connell, P.E., 2008. RainSim: a spatial temporal stochastic rainfall modelling system. Environ. Modell. Softw. 23 (12), 1356–1369. http://dx.doi.org/10.1016/j.envsoft.2008.04.003.

Burton, A., Fowler, H.J., Blenkinsop, S., Kilsby, C.G., 2010. Downscaling transient climate change using a Neyman–Scott rectangular pulses stochastic rainfall model. J. Hydrol. 381, 18–32. http://dx.doi.org/10.1016/j.jhydrol.2009.10.031.

Christensen, J.H., Hewitson, B., Busuioc, A., Chen, A., Gao, X., Held, I., Jones, R., Kolli, R.K., Kwon, W.-T., Laprise, R., Magaña Rueda, V., Mearns, L., Menéndez, C.G., Räisänen, J., Rinke, A., Sarr, A., Whetton, P., 2007. Regional climate projections. In: Solomon, S., Qin, D., Manning, M., Chen, Z., Marquis, M., Averyt, K.B., Tignor, M., Miller, H.L. (Eds.), Climate Change 2007: The Physical Science Basis. Contribution of Working Group I to the Fourth Assessment Report of the Intergovernmental Panel on Climate Change. Cambridge University Press, Cambridge, United Kingdom and New York, NY, USA.

Dee, D.P., Uppala, S.M., Simmons, A.J., Berrisford, P., Poli, P., Kobayashi, S., Andrae, U., Balmaseda, M.A., Balsamo, G., Bauer, P., Bechtold, P., Beljaars, A.C.M., van de Berg, L., Bidlot, J., Bormann, N., Delsol, C., Dragani, R., Fuentes, M., Geer, A.J., Haimberger, L., Healy, S.B., Hersbach, H., Holm, E.V., Isaksen, L., Kallberg, P., Kohler, M., Matricardi, M., McNally, A.P., Monge-Sanz, B.M., Morcrette, J.-J., Park, B.-K., Peubey, C., de Rosnay, P., Tavolato, C., Thepaut, J.-N., Vitart, F., 2011. The ERA-Interim reanalysis: configuration and performance of the data assimilation system. Q. J. Roy. Meteorol. Soc. 137 (656), 553–597. http://dx.doi.org/10.1002/qj.828.

Diaz-Nieto, J., Wilby, R.L., 2005. A comparison of statistical downscaling and climate change factor methods: impacts on low flows in the River Thames, United Kingdom. Climatic Change 69 (2–3), 245–268. http://dx.doi.org/10.1007/s10584-005-1157-6.

Ehret, U., Zehe, E., Wulfmeyer, V., Warrach-Sagi, K., Liebert, J., 2012. HESS opinions: "should we apply bias correction to global and regional climate model data?". Hydrol. Earth Syst. Sci. 16 (9), 3391–3404. http://dx.doi.org/10.5194/hess-16-3391-2012.

Forsythe, N., Fowler, H.J., Kilsby, C.G., Archer, D.R., 2012a. Opportunities from remote sensing for supporting water resources management in village/valley scale catchments in the Upper Indus Basin. Water Resour. Manage. 26 (4), 845–871. http://dx.doi.org/10.1007/s11269-011-9933-8.

Forsythe, N., Kilsby, C.G., Fowler, H.J., Archer, D.R., 2012b. Assessment of runoff sensitivity in the Upper Indus Basin to interannual climate variability and potential change using MODIS satellite data products. Mountain Res. Dev. 32 (1), 16–29. http://dx.doi.org/10.1659/MRD-JOURNAL-D-11-00027.1.

Fowler, H.J., Archer, D.R., 2006. Conflicting Signals of Climate Change in the Upper Indus Basin. J. Climate 19 (17), 4276–4292. http://dx.doi.org/10.1175/JCLI3860.1.

Fowler, H.J., Blenkinsop, S., Tebaldi, C., 2007. Linking climate change modelling to impacts studies: recent advances in downscaling techniques for hydrological modelling. Int. J. Climatol. 27 (12), 1547–1578. http://dx.doi.org/10.1002/joc.1556.

Gardelle, J., Berthier, E., Arnaud, Y., 2012. Contrasting patterns of early twenty-first-century glacier mass change in the Himalayas. Nature Geosci. 5 (5), 322–325. http://dx.doi.org/10.1038/ngeo1450.

Goderniaux, P., Brouyére, S., Blenkinsop, S., Burton, A., Fowler, H.J., Orban, P., Dassargues, A., 2011. Modeling climate change impacts on groundwater resources using transient stochastic climatic scenarios. Water Resour. Res. 47 (12). http://dx.doi.org/10.1029/2010WR010082. Art. no. W12516.

Hashmi, A.A., Shafiullah, 2003. NASSD background paper: agriculture and food security. IUCN Pakistan, Northern Areas Progamme, Gilgit, pp. x + 136. ISBN: 969-8141-42-1. <http://cmsdata.iucn.org/downloads/bp_agri_fo_sec.pdf> (accessed 17.04.13).

Immerzeel, W.W., Droogers, P., de Jong, S.M., Bierkens, M.F.P., 2008. Large-scale monitoring of snow cover and runoff simulation in Himalayan river basins using remote sensing. Remote Sens. Environ. 113 (1), 40–49. http://dx.doi.org/10.1016/j.rse.2008.08.010.

IPCC SRES, 2000. In: Nakicenovic, N., Swart, R. (Eds.), Special Report on Emissions Scenarios: A special report of Working Group III of the Intergovernmental Panel on Climate Change. Cambridge University Press, ISBN 0-521-80081-1, 978-052180081-5.

Jacob, D., Bärring, L., Christensen, O.B., Christensen, J.H., De Castro, M., Déqué, M., Giorgi, F., Hagemann, S., Hirschi, M., Jones, R., Kjellström, E., Lenderink, G., Rockel, B., Sánchez, E., Schär, C., Seneviratne, S.I., Somot, S., Van Ulden, A., Van

Den Hurk, . An inter-comparison of regional climate models for Europe: model performance in present-day climate. Climatic Change 81 (1, Suppl. 1), 31–52. http://dx.doi.org/10.1007/s10584-006-9213-4.

Jacob, T., Wahr, J., Pfeffer, T.W., Swenson, S., 2012. Recent contributions of glaciers and ice caps to sea level rise. Nature 482, 514–518. http://dx.doi.org/10.1038/nature10847.

Jones, P.D., Harpham, C., Goodess, C.M., Kilsby, C.G., 2011. Perturbing a weather generator using change factors derived from regional climate model simulations, Nonlin. Process. Geophys. 18, 503–511. http://dx.doi.org/10.5194/npg-18-503-2011.

Jones, P.D., Kilsby, C.G., Harpham, C., Glenis, V., Burton, A., 2009. UK Climate Projections Science Report: Projections of Future Daily Climate for the UK from the Weather Generator. University of Newcastle, UK.

Jones, R.G., Noguer, M., Hassell, D.C., Hudson, D., Wilson, S.S., Jenkins, G.J., Mitchell, J.F.B., 2004. Generating High Resolution Climate Change Scenarios using PRECIS. Met Office Hadley Centre, Exeter, UK, p. 40, http://www.metoffice.gov.uk/media/pdf/6/5/PRECIS_Handbook.pdf.

Kilsby, C.G., Jones, P.D., Burton, A., Ford, A.C., Fowler, H.J., Harpham, C., James, P., Smith, A., Wilby, R.L., 2007. A daily weather generator for use in climate change studies. Environ. Modell. Softw. 22 (12), 1705–1719. http://dx.doi.org/10.1016/j.envsoft.2007.02.005.

KNMI: Project team ECA&D, Royal Netherlands Meteorological Institute, 2012. European Climate Assessment & Dataset (ECA&D) Algorithm Theoretical Basis Document (ATBD) [Project Number: EPJ029135] Version 10.6. <http://eca.knmi.nl/documents/atbd.pdf> (accessed 16.04.13).

Liang, X.-Z., Kunkel, K.E., Meehl, G.A., Jones, R.G., Wang, J.X.L., 2008. Regional climate models downscaling analysis of general circulation models present climate biases propagation into future change projections. Geophys. Res. Lett. 35 (8), L08709. http://dx.doi.org/10.1029/2007GL032849.

Mathison, C., Wiltshire, A., Dimri, A.P., Falloon, P., Jacob, D., Kumar, P., Moors, E., Ridley, J., Siderius, C., Stoffel, M., Yasunari, T., 2014. Regional projections of North Indian climate for adaptation studies. Sci. Tot. Environ. 468–469, S4–S17. http://dx.doi.org/10.1016/j.scitotenv.2012.04.066.

Ozturk, T., Altinsoy, H., Turkes, M., Kurnaz, M.L., 2012. Simulation of temperature and precipitation climatology for the Central Asia CORDEX domain using RegCM 4.0. Climate Res. 52, 63–76. http://dx.doi.org/10.3354/cr01082.

Pan, Z., Christensen, J.H., Arritt, R.W., Gutowski Jr., W.J., Takle, E.S., Otieno, F., 2001. Evaluation of uncertainties in regional climate change simulations. J. Geophys. Res. D: Atmos. 106 (D16), 17735–17751. http://dx.doi.org/10.1029/2001JD900193.

Peters, G.P., Andrew, R.M., Boden, T., Canadell, J.G., Ciais, P., Le Quéré, C., Marland, G., Raupach, M.R., Wilson, C., 2013. The challenge to keep global warming below 2 C. Nat. Climate Change 3 (1), 4–6. http://dx.doi.org/10.1038/nclimate1783.

Pope, V.D., Gallani, M.L., Rowntree, P.R., Stratton, R.A., 2000. The impact of new physical parameterizations in the Hadley Centre climate model: HadAM3. Climate Dyn. 16 (2–3), 123–146. http://dx.doi.org/10.1007/s003820050009.

Rangwala, I., Miller, J.R., 2012. Climate change in mountains: a review of elevation-dependent warming and its possible causes. Climatic Change 114 (3-4), 527–547. http://dx.doi.org/10.1007/s10584-012-0419-3.

Rangwala, I., Miller, J.R., Russell, G.L., Ming, X., 2010. Using a global climate model to evaluate the influence of water vapor, snow cover and atmospheric aerosol on warming in the Tibetan Plateau during the twenty-first century. Climate Dyn. 34 (6), 859–872. http://dx.doi.org/10.1007/s00382-009-0564-1.

Rummukainen, M., 2010. State-of-the-art with regional climate models. WIREs Climate Change 1, 82–96. http://dx.doi.org/10.1002/wcc.008.

Sharif, M., Archer, D.R., Fowler, H.J., Forsythe, N., 2013. Trends in timing and magnitude of flow in the Upper Indus Basin. Hydrol. Earth Syst. Sci. 17 (4), 1503–1516. http://dx.doi.org/10.5194/hess-17-1503-2013.

Singh, P., Kumar, N., Arora, M., 2000. Degree-day factors for snow and ice for Dokriani Glacier, Garhwal Himalayas. J. Hydrol. 235 (1–2), 1–11. http://dx.doi.org/10.1016/S0022-1694(00)00249-3.

Spencer, H., Slingo, J.M., 2003. The simulation of peak and delayed ENSO teleconnections. J. Climate 16 (11), 1757–1774. http://dx.doi.org/10.1175/1520-0442(2003)016<1757:TSOPAD>2.0.CO;2.

Uppala, S.M., Kallberg, P.W., Simmons, A.J., Andrae, U., Da Costa Bechtold, V., Fiorino, M., Gibson, J.K., Haseler, J., Hernandez, A., Kelly, G.A., Li, X., Onogi, K., Saarinen, S., Sokka, N., Allan, R.P., Andersson, E., Arpe, K., Balmaseda, M.A., Beljaars, A.C.M., Vande Berg, L., Bidlot, J., Bormann, N., Caires, S., Chevallier, F., Dethof, A., Dragosavac, M., Fisher, M., Fuentes, M., Hagemann, S., Holm, E., Hoskins, B.J., Isaksen, L., Janssen, P.A.E.M., Jenne, R., McNally, A.P., Mahfouf, J.-F., Morcrette, J.-J., Rayner, N.A., Saunders, R.W., Simon, P., Sterl, A., Trenberth, K.E., Untch, A., Vasiljevic, D., Viterbo, P., Woollen, J., 2005. The ERA-40 re-analysis. Quart. J. Roy. Meteorol. Soc. 131 (612), 2961–3012. http://dx.doi.org/10.1256/qj.04.176.

van Vliet, M.T.H., Blenkinsop, S., Burton, A., Harpham, C., Broers, H.P., Fowler, H.J., 2012. A multi-model ensemble of downscaled spatial climate change scenarios for the Dommel catchment, Western Europe. Climatic Change 111 (2), 249–277. http://dx.doi.org/10.1007/s10584-011-0131-8.

Visser, A., Kroes, J., van Vliet, M., Blenkinsop, S., Fowler, H.J., Broers, H.P., 2012. Climate change impacts on the leaching of a heavy metal contamination in a small lowland catchment. J. Contam. Hydrol. 127 (1–4), 47–64.

Wetherald, R.T., Manabe, S., 2002. Simulation of hydrologic changes associated with global warming. J. Geophys. Res. D: Atmos. 107 (19), XXI–XXII. http://dx.doi.org/10.1029/2001JD001195.

Wijngaard, J.B., Klein Tank, A.M.G., Können, G.P., 2003. Homogeneity of 20th century European daily temperature and precipitation series. Int. J. Climatol. 23 (6), 679–692. http://dx.doi.org/10.1002/joc.906.